Free-electron-laser oscillator with a linear taper

A. Christodoulou, D. Lampiris, K. Polykandriotis, W. B. Colson, and P. P. Crooker
Naval Postgraduate School, Monterey, California 93943

S. Benson, J. Gubeli, and G. R. Neil
Thomas Jefferson National Accelerator Facility, Newport News, Virginia 23606
(Received 2 April 2002; published 11 November 2002)

We present experiments and simulations showing the behavior of a free-electron laser (FEL) with both positive and negative linear tapers along the wiggler. We show the power desynchronism curve widths, efficiency, exhaust electron energy spread, and wavelength dependence as a function of taper for 3- and 6-μm optical wavelengths and for resonators with 10% and 2% loss/pass. Simulations of the experiments, using a multimode analysis, are seen to be in general agreement with the experimental results, carried out at the IR Demo FEL at Thomas Jefferson National Accelerator Facility. We find that short-pulse effects are more effective than tapers in producing high efficiency with low exhaust energy spread, and the expected performance enhancement of FEL tapering is not achieved.

DOI: 10.1103/PhysRevE.66.056502 PACS number(s): 41.60.Cr

INTRODUCTION

In the early days of free-electron lasers (FEL's), variable parameter wigglers were suggested to enhance the efficiency of FEL's [1]. One way to achieve this is through wiggler tapering, in which the magnetic field decreases (referred to as positive taper) or increases (referred to as negative or inverse taper) along the wiggler axis. A theory for tapered wigglers, proposed by Kroll, Morton, and Rosenbluth [2], assumes a single-frequency plane-wave input and is thus applicable to FEL amplifiers. Application of the theory to an inverse taper [3] (or ''phase displacement'') also assumes a plane wave, though pulsed effects have been considered. The two schemes share a common theoretical feature, namely a well-defined ponderomotive potential as an initial condition. Early tapered oscillators used a multicomponent design in order to enhance the small-signal gain at the frequency necessary to extract energy from the electrons and produce a good trapping fraction [4]. In an early experiment, researchers at Los Alamos National Laboratory reported the characteristics of a wavelength-tapered wiggler at high optical power [5]. In 1995, experimental studies at FELIX and Orsay [6] and theoretical studies by Saldin, Schneidmiller, and Yurkov [7] (SSY) showed that a mild negative taper should produce better extraction efficiency than a positive taper. For the case of a positively tapered wiggler, there is a mismatch between the optimal frequency for small-signal gain and the optimal frequency for saturated lasing. There is no such mismatch for an oscillator with a mild *inverse* taper, allowing it to start up more efficiently.

The analysis by SSY provided the original motivation to look at the effect of tapering on the IR Demo FEL [8] at Jefferson Laboratory. One can easily create a taper in a hybrid permanent magnet wiggler by introducing a linear gap change along the wiggler. The field taper is very nearly linear and the magnetic-field quality is still excellent. However, there are important differences between the SSY theory and our experiments. First, SSY assume a single frequency, while the IR Demo FEL utilizes short, multifrequency electron pulses and operates in the short optical pulse regime. In this regime, the FEL develops a short optical pulse that passes over the electron pulse as they both travel through the wiggler. An electron, therefore, effectively sees a shorter interaction length, which is equivalent to a shorter wiggler. The efficiency of the untapered FEL is therefore enhanced due to the smaller number of effective wiggler periods (the efficiency is inversely proportional to the number of wiggler periods for an untapered wiggler), while the tapered operation is degraded since the electrons do not see the full taper during the time that the optical field is present.

A second difference between SSY and our experiments is that our resonator losses are higher than those used by SSY. Higher losses should result in lower efficiencies for the IR Demo for most tapers. We therefore analyze our data using simulations that incorporate a multimode analysis to take account of the laser pulses, and resonator losses corresponding to those of our experiment.

Since the IR Demo FEL utilizes energy recovery, the overall performance is sensitive to the *total* electron energy spread at the output of the FEL wiggler. Experiments with step-tapered oscillators have indicated that the root-mean-square (rms) energy spread is smaller for an inverse step taper than for an untapered FEL for the same efficiency. We were therefore quite interested to see if an inverse linear taper could provide enhanced efficiency while maintaining or even decreasing the total exhaust energy spread.

EXPERIMENT

The IR Demo FEL and accelerator, described in detail previously [8], is shown in Fig. 1. It has $N=41$ wiggler periods of length $\lambda_0=2.7$ cm each, a wiggler parameter $K=eB_{\rm rms}\lambda_0/(2\pi mc^2)=0.98$, and is operated with $\approx$0.8 ps [full width at half maximum (FWHM)] electron micropulses (pulse length $l_e\approx 230\ \mu$m) with peak current $I\approx 60$ A. The taper is contained in the pendulum equation torque $\delta=-[4\pi NK^2/(1+K^2)]\ (\Delta K/K)$.

Two experimental runs with the laser were carried out. In

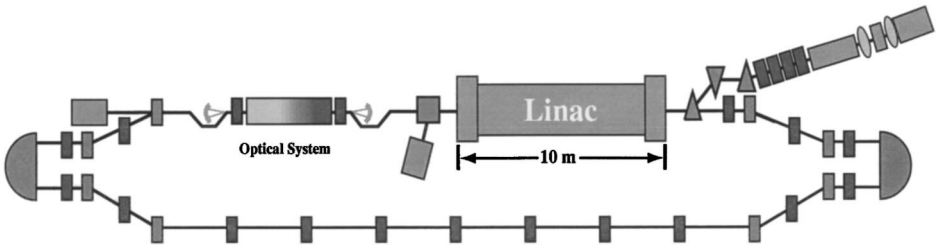

FIG. 1. Schematic diagram of the TJNAF IR Demo FEL. The injector (upper right) feeds electrons through a linac into the wiggler (optical system) where lasing takes place. The electron beam is then recirculated along the bottom path.

the first, the laser was operated at wavelengths near $\lambda = 3\ \mu$m with a resonator having 10% energy loss per round-trip pass of a pulse. Untapered operation and three tapers of both signs were studied: $\delta = 0, \pm 4\pi, \pm 6\pi, \pm 8\pi$. Exhaust energy profiles were obtained by looking at a viewer downstream of the FEL when lasing with a pulsed beam. In the second set of experiments, the laser was operated near 6 μm with 10% loss/pass and $\delta = 0$, $\pm 4\pi$, and -8π. Finally, with the laser wavelength still set at 6 μm, the cavity losses were adjusted to 2% and tapers of -7π and $+10\pi$ were studied. In each case, slit scans of the electron beam were utilized to measure the electron-beam exhaust energy spread.

For each taper, the laser was optimized with pulsed lasing conditions. Typically the macropulses were 1 ms long at 60 Hz. At this power level, slightly higher electron losses could be tolerated and mirror-heating effects were negligible compared to CW operation. With almost 19 000 cavity round trips during the macropulse, the laser had plenty of time to reach an equilibrium state. For a certain cavity length S, referred to as the *synchronous length*, the electron and optical pulses are in perfect synchronism as they enter the wiggler. Changing the cavity length by ΔS from the synchronous length causes the optical and electron pulses to desynchronize. The average power is measured as a function of the desynchronism $d = 2\Delta S/N\lambda$. For each taper, spectra at the peak of the desynchronism curve and at $\frac{1}{3}$ and $\frac{2}{3}$ of the way out on the curve were measured. Finally, the CW lasing performance was optimized and measured.

Tapers were obtained by inserting precision shims at either end of the wiggler. Dial gauges on either side of the wiggler measured the position and gap of the wiggler for each taper. Since the variation of the wiggler field with gap size is known, the field taper can be calculated from the gap taper. For a field taper of only 10%, a linear taper is an excellent approximation to the real variation. The resonant energy prediction will differ by less than 0.1% from the actual resonant energy for a resonant energy taper of 5% (corresponding to 10% field taper).

SIMULATION TECHNIQUE

Computer simulations were performed using the self-consistent Maxwell-Lorentz equations [9] and dimensionless parameters derived from the Thomas Jefferson National Accelerator Facility (TJNAF) FEL experimental parameters. The wiggler parameter $K = 0.98$ has been given above. For $\lambda = 3\ \mu$m, the dimensionless current is $j = 8N(\pi eKN\lambda_0)^2\rho F/(\gamma^3 mc^2) = 7$, where ρ is the electron-beam density, and the filling factor F is the ratio of the areas of the electron and optical beams. While the charge per micropulse is known to a few percent, the details of the electron pulse shape and hence the peak current are uncertain. The electron pulse shape was therefore taken to be parabolic, described by $j(z) = j(1 - 2z^2/\sigma_z^2)$, where $z = z_{\text{actual}}/N\lambda$ and $\sigma_z = l_e/N\lambda = 1.8$. For $\lambda = 6\ \mu$m, $j = 10$ and $\sigma_z = 1$. To provide perspective, weak-field gain is estimated by $G = \Delta P/P = 0.135j$, where $\Delta P/P$ is the fractional increase in the optical power during one pass through the undulator. The resonator losses, determined by the total loss per pass from the resonator mirrors, are either 10% or 2%; the desynchronism d is varied from 0 to 0.4.

In dimensionless notation, the electron phase velocity is given by

$$\nu = 2\pi N\left[1 - \frac{(1+K^2)\lambda_0}{2\gamma^2\lambda}\right], \tag{1}$$

where $N = 41$ is the number of wiggler periods and γ is the relativistic Lorentz factor. The phase velocity is the meeting point between the dimensionless simulations and experiment.

Since the IR Demo FEL has a micropulse structure, the behavior was simulated by introducing a short electron pulse into the optical resonator and examining the evolution of the pulse and the optical mode as a function of the number of round trips n the pulse has made through the resonator. Figure 2 shows the output for a typical simulation run, in this case the behavior after 6000 passes through a wiggler with positive taper ($\delta = 6\pi$). The upper graphs give the shape of several dimensionless quantities: the optical field $|a(z,n)|$, the optical power spectrum $P(\nu,n)$, and the electron spectrum $f(\nu,n)$, all at the end of the final pass. The shading in the middle graphs shows how these quantities have evolved with the number of passes n. On the bottom left, the longitudinal pulse shape of the current density $j(z-\tau)$ is shown for dimensionless times $\tau = 0$ and 1, corresponding to one pass through the wiggler. As noted above, this pulse shape is not actually known, and we choose an inverted parabolic shape for convenience. The bottom center graph shows the weak-field gain spectrum, and the right-hand bottom graph can be configured to show the evolution of either the dimensionless total power P (proportional to the integrated dimensionless electric field squared [9]) or the gain G as a function of n. The dimensionless parameters printed across the top are the peak current j, the fractional energy loss per round trip

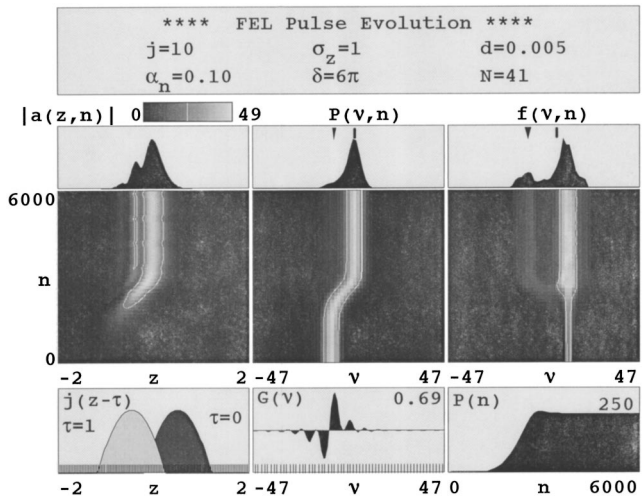

FIG. 2. Simulation results for pulsed-laser operation. See text for explanation.

α_n, the pulse width σ_z, the taper rate δ, the desynchronism d, and the number of wiggler periods N. In addition to showing many interesting details of the behavior, the simulations can also print out the final power P_f or the gain G, both of which are strong functions of desynchronism. Also printed are the efficiency $\eta=\langle\Delta\gamma mc^2\rangle/\gamma mc^2$ and the phase velocity at the peak of the optical spectrum. These quantities provide a good general assessment of the effect of taper on FEL behavior.

Note that we start the simulation with the electrons at an initial phase velocity ν_0 corresponding to the peak of the weak-field gain spectrum. Since, however, the gain spectrum is a function of the field amplitude, the optical power shifts to other values of ν as the field grows, as shown in the center panel of Fig. 2.

Figures 3 and 4 show the results of many simulation runs for $j=7$, $\lambda=3\ \mu$m, and 10% loss/pass. Figure 3 shows the weak-field multimode gain versus desynchronism d while the optical field is still weak and the power is increasing. The upper graph shows negative tapers; the lower graph shows positive tapers. As expected from theory [7], the gain is essentially independent of the sign of the taper.

The FEL oscillator operates above threshold when the gain/pass exceeds the loss/pass, shown by the dotted line at 10% in Fig. 3. When the gain exceeds the loss, the optical power grows over many passes to saturation in strong fields. Once the laser power reaches saturation, the net gain becomes zero. Figure 4 shows the resulting average saturated power, also as a function of desynchronism and taper. Similar graphs are obtained for $\lambda=6\ \mu$m, 10% loss/pass and for $\lambda=6\ \mu$m, 2% loss/pass.

One general feature of Figs. 3 and 4 is that the gain and the desynchronism operating range decrease as the taper rate δ increases in magnitude. The operating range is also a function of dimensionless current j; for example, if $j=6$ and $\delta=\pm 8\pi$ (not shown), the laser will not work at all. In the start-up region where d is small, the number of passes n required to achieve the final power is large, but for larger d, where the gain is also larger, the number of passes is greatly

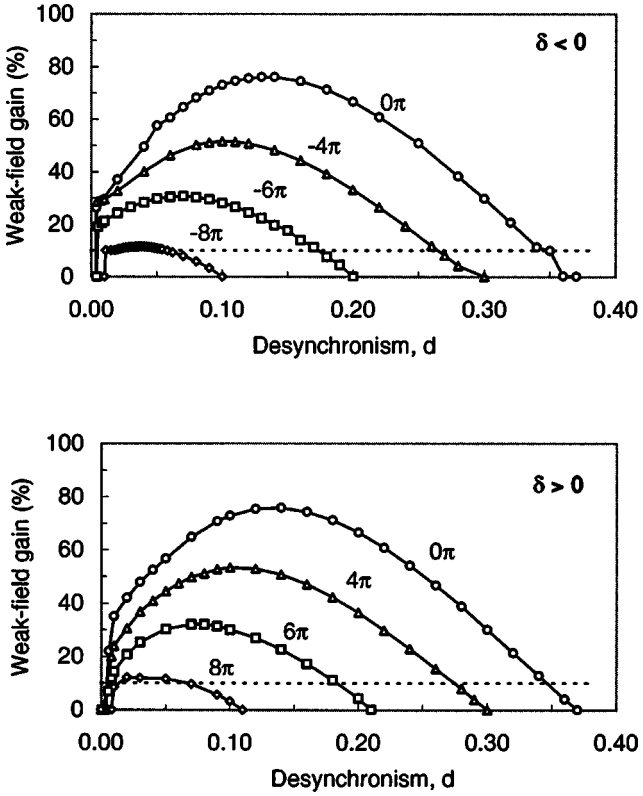

FIG. 3. Weak-field gain vs desynchronism for $j=7$, $\lambda=3\ \mu$m. Top: negative taper ($\delta=0--8\pi$); bottom: positive taper ($\delta=0-8\pi$). The width of the power vs desynchronism curve is determined by the point where the gain curve crosses the 10% cavity loss/pass threshold.

reduced. For $\delta=0$ and negative tapers, the sharp peaks in power are accompanied by evidence of the trapped-particle instability. This effect is reduced for positive tapers and vanishes for $\delta=8\pi$. The instability is caused by electrons in the presence of strong optical fields becoming trapped in potential wells in phase space and oscillating at the trapped-particle synchrotron frequency $\nu_s=(|a|^2-\delta^2)^{1/4}$ [9].

When $d<0.1$, the final power, gain, and electron spectrum may oscillate regularly, in some cases exhibiting up to 50% modulation of the average power over hundreds of wiggler passes. For these regions, shown by the open circles on the power curves in Fig. 4, only the average values of the steady-state power are shown. We attribute these nonsteady effects to limit-cycle behavior [10], caused by the trapped particle instability combined with short optical pulses. The modulation, caused by the oscillation of the trapped current, continually modifies the shape of the short optical pulse. The different pulse shapes have different powers and spectra, causing oscillations as subpulse structures ''march'' through the pulse envelope.

In the simulations, the desynchronism curves are qualitatively different for positive and negative tapers. For positive δ, the power curves flatten, with the power diminishing significantly as the taper increases. For negative δ, the curves have a more triangular shape. Note that the untapered power exceeds the positively tapered power for most of the range of d. For $\delta=-4\pi$, however, tapering provides power greater

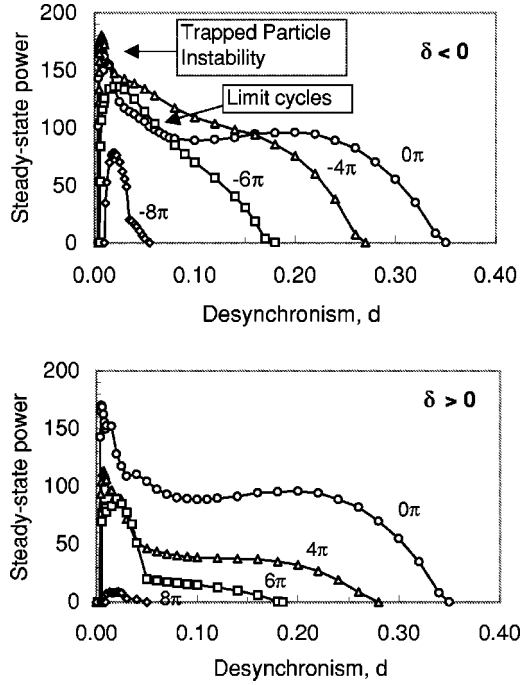

FIG. 4. Dimensionless saturated power vs desynchronism for $j=7$, $\lambda=3\,\mu$m. Top: negative taper ($\delta=0--8\pi$); bottom: positive taper ($\delta=0-8\pi$). The trapped particle and limit cycle regions are discussed in the text.

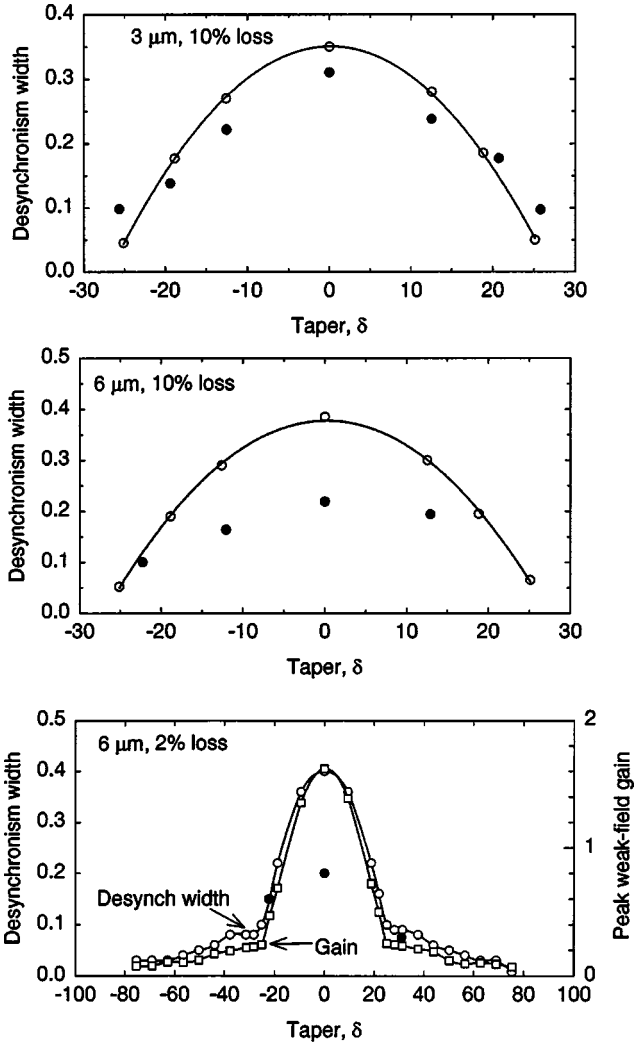

FIG. 5. Total width of the desynchronism curves vs taper. Solid circles are experimental; open circles are simulations. For 10% loss/pass, the solid curve is a quadratic fit to the simulations and is provided as a guide to the eye. For 2% loss/pass, the gain switches to a different peak on the weak-field gain curve $G(\nu)$ near $|\delta|=8\pi$, as shown by both the gain and desynchronism width.

than the untapered case up to $d=0.18$, while for $\delta=-6\pi$ the improvement ends at $d=0.09$.

EXPERIMENTAL RESULTS AND DISCUSSION

In general, wiggler taper decreases the weak-field gain and the width of both the power and gain desynchronism curves, as shown in Figs. 3 and 4. Figure 5 shows the total widths of the power desynchronism curves versus taper δ for both experiment (solid circles) and simulation (open circles) at wavelengths $\lambda=3$ and 6 μm. For 10% loss/pass, the simulation points are arbitrarily fit with parabolas, presented merely as a guide to the eye. Their purpose is to show that, as expected from theory, the desynchronism width tends to be symmetrical about $\delta=0$. The experimental data follow this trend, and the agreement is reasonable.

For 2% loss/pass, the simulations were expanded to larger values of δ in order to explain the data. Here the gain per pass is significantly more than the loss per pass, which increases the widths of the power desynchronism curves compared to the case of 10% loss/pass. For $|\delta|<8\pi$, the desynchronism width is approximately parabolic in δ, decreasing from $d=0.4$ at $\delta=0$ to $d=0.1$ near $|\delta|=8\pi$. At $|\delta|\approx 8\pi$, however, the slope of the curve decreases significantly. Beyond $|\delta|\approx 8\pi$, the width decreases linearly with δ.

The cause of this behavior lies in the dependence of the weak-field gain spectrum on δ (see the lower center panel of Fig. 2). As δ increases, the gain in the primary peak decreases while a secondary peak grows over the same range. For $|\delta|>8\pi$, the original secondary peak becomes the primary peak and the original primary peak decreases to negligible levels. The new primary peak has a different dependence on δ. To show the dependence of the desynchronism width on the gain, Fig. 5 also shows the peak gain (i.e., the peak of the gain curves as shown in Fig. 3) versus δ. As one can see, there is a clear correspondence between the desynchronism curve width and peak gain.

Note that the experimental desynchronism widths are now in agreement with the simulations in the wings of Fig. 5 but not for $\delta=0$. We believe the cause lies in focusing effects for $\delta=0$ as previously described by Benson *et al.* [11].

The peak efficiency, defined as the emitted optical power divided by the incident electron beam power, is shown versus taper in Fig. 6 for both pulsed and CW operation. For the multimode operation described here, the simulations show that increasing the magnitude of the taper causes the efficiency to decrease for both high and low loss/pass. The experiments agree with the simulations for $\lambda=3\,\mu$m, but at $\lambda=6\,\mu$m the simulations show higher efficiency than the

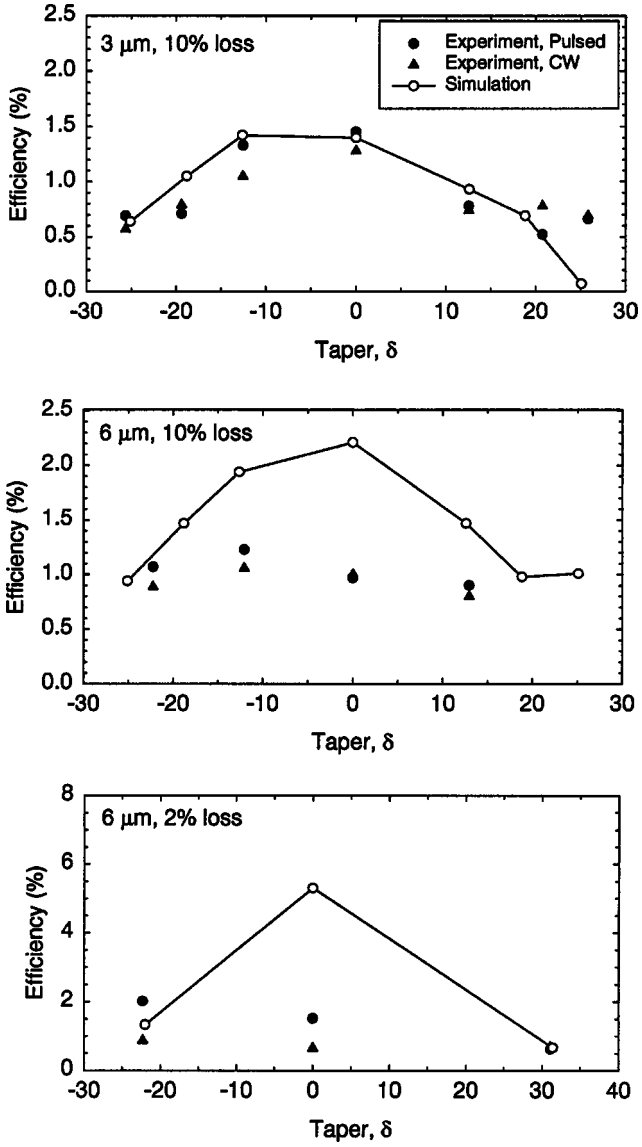

FIG. 6. FEL efficiency vs taper. Solid circles are the experiment: circles for pulsed operation, triangles for CW operation. The open circles are the simulation. The lines are a guide to the eye.

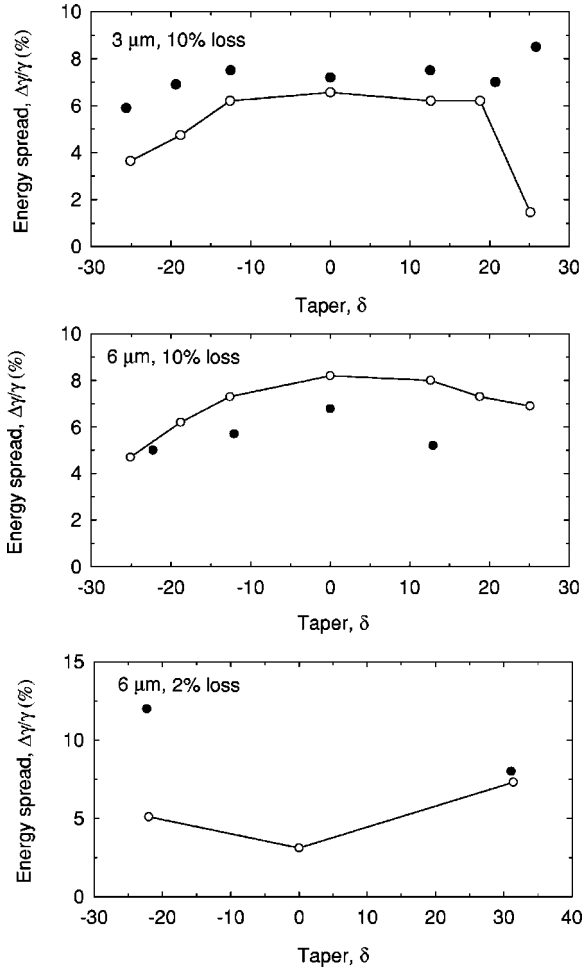

FIG. 7. Energy spread of the exhaust electrons vs taper. Solid circles are experiment; open connected dots are the simulation. The energy spread determined from the simulation is $\Delta\nu/4\pi N$, where $\Delta\nu$ is the total width of the electron spectrum $f(\nu,n)$.

experiments when the taper is small. It is not clear why this is so. It may have to do with the micropulse shape, which may have been different for the two wavelengths.

The efficiency for the case of 2% loss/pass and no taper was surprisingly low in the experiments. Higher efficiency was limited by the inability to recirculate the beam due to the occasional strong lasing accompanied by a large exhaust energy spread. At 2% loss/pass and small values of desynchronism ($d=0.002$), the FEL reaches high optical power, which induces a large electron beam energy spread $\Delta\gamma/\gamma\approx 15\%$. Such a large energy spread causes the accelerator to shut down, so that larger desynchronism values are often selected for stable operation. While the simulations do not cause shut down, they do show correspondingly large energy spread.

Figure 7 shows the full width fractional energy spread $\Delta\gamma/\gamma$ of the exhaust electrons at the peak of the desynchronism curve versus taper δ. Single-mode simulations have shown that an inverse taper has a smaller energy spread at the FEL exit, and the multimode simulations of Fig. 7 bear this out. The effect is not large, however. In general, one expects $\Delta\gamma/\gamma$ to be largest at the largest efficiency where there is the most trapping near zero taper. For 10% loss/pass, the experiment and theory are in reasonable agreement, except for $\lambda=3$ μm near $\delta=25$. Here the simulations indicate very little trapping, while the experimental spreads are over five times larger and indicate that, at least part of the time, the laser field does trap and decelerate some electrons. For 2% loss/pass, we have only two experimental points. At large positive taper, the agreement is good, but at large negative taper, the experimental spread is twice the theoretical spread.

The experimental electron distributions for positive taper, negative taper, and no taper looked qualitatively different. Slit scans and viewer images were taken at a dispersed location to study the distributions and it was found that the untapered case has a nearly top hat distribution. In general, the energy distributions varied with cavity length and degree of taper. The general trend was for the positive taper to have a low-energy tail and the negative taper to have a high-energy tail and very sharp low-energy edge. The positive taper typi-

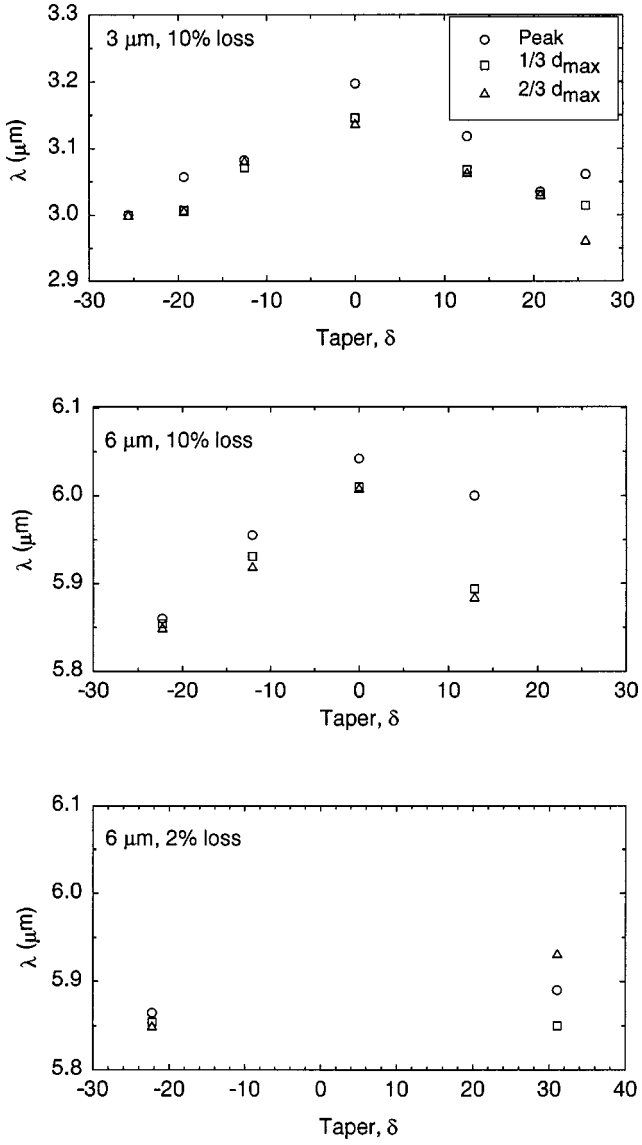

FIG. 8. Experimental wavelength vs taper. Wavelengths are taken from three points on the power desynchronization curve: at the peak power, $\frac{1}{3}$ of $d_{\max}$, and $\frac{2}{3}$ of $d_{\max}$.

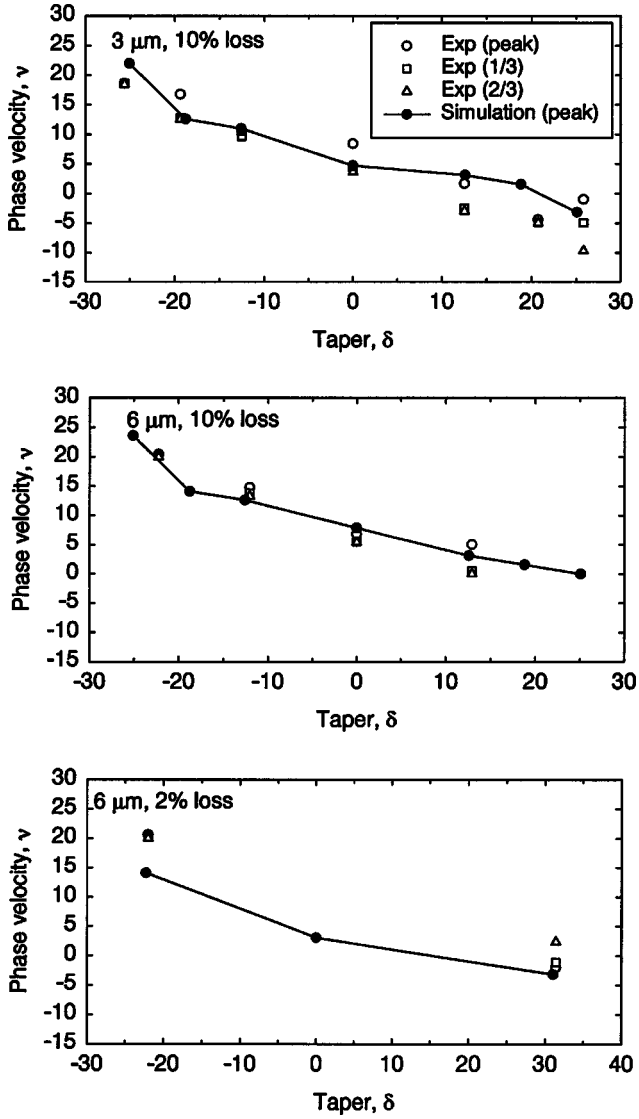

FIG. 9. Phase velocity ν for the data of Fig. 8 vs taper. The experimental values are calculated from Eq. (1) as described in the text. Simulation values are from the peak of the optical spectrum $P(\nu,n)$.

cally has a double-humped distribution with a decelerated bucket and a second peak corresponding to the untrapped electrons. Electron distributions were also examined in the simulations, but, unlike the experimental case, no systematic dependence of the distribution on taper could be made.

In order to adjust the taper on the FEL, it is necessary to increase the spacing of one or the other ends of the wiggler to create a wiggler gap variation. In addition to creating taper, however, the average magnetic field of the wiggler is correspondingly lowered, which lowers the operating wavelength of the FEL. Figure 8 shows the experimental wavelengths versus taper; note that in all cases the wavelength decreases when taper is introduced, as would be expected.

A comparison of these data with the simulations can be accomplished through the phase velocity ν. As shown in Eq. (1), the experimental parameters can be combined to produce an experimental phase velocity, which is then compared with the phase velocity produced by the simulations. For constant electron energy γ and wiggler period λ_0, ν depends on optical wavelength λ and wiggler parameter K, both of which change when the taper is changed in the experiment. We therefore calculate the phase velocity corresponding to the various experimental values of λ and K and compare them to the values obtained by simulation. The results are shown in Fig. 9, where for the experimental ν we have used values of λ, λ_0, γ, and K that are well within the experimental uncertainties, and have corrected for the Guoy phase shift in the resonator. Note that the general trend of the phase velocity is to shift monotonically from above to below resonance ($\nu=0$) as the taper is increased. This behavior is described by the theoretical dependence [9] of the gain spectrum on δ, according to $\nu_{\text{peak}}=\nu_1-\delta/2$. For weak fields, $\nu_1=2.6$; for the moderate fields utilized here, $\nu_1\approx 5$. We find that the agreement is quite good. Evidently the saturated frequency

remains near the small-signal frequency, which in turn means that the optical fields are not sufficient to strongly trap and decelerate electrons.

CONCLUSIONS

These experiments and simulations provide a good general idea of the effect of taper on FEL performance under conditions of high power and pulsed output. For 10% loss/pass, agreement between experiment and theory is reasonably good, while for 2% loss/pass there appear to be gaps in our understanding. Beginning with the high loss/pass results, we first find that the width of the power desynchronism curve generally decreases with increasing taper and is independent of the sign of the taper. Next, we find that the efficiency is also decreased by taper of either sign, at least for $\lambda = 3\ \mu$m, which is due to decreased trapping. For $\lambda = 6\ \mu$m, the experimental efficiency turns out to be only weakly dependent on the taper, in contrast to the 6-μm simulations, which behave similarly to the 3-μm case. The cause of this behavior is not clear and we have not been able to reconcile this difference.

The energy spread of the exhaust electrons is of great interest for a recirculating FEL. Under pulsed conditions, both experiment and simulations show that the energy spread decreases with a taper of either sign, but not by very much. The exception is for a large positive taper where the experimental energy spread increases, while the simulations show a large decrease. Presumably this is because there is still trapping in the experiment, while the simulations show that the trapping is greatly decreased.

Adjusting the taper of the IR Demo FEL necessitates a change in the wiggler parameter K, thereby causing a corresponding decrease in λ for a taper of either sign. Expressing these results as changes in an experimental phase velocity ν, we find that the results agree well with the simulations. Both show that the wavelength tends to be close to the small-signal wavelength. This effect leads to the poor performance of the positively tapered oscillator.

The most important conclusion is that short-pulse effects are much more effective than taper in producing high efficiency with low exhaust energy spread. The short pulses do not allow a stable ponderomotive potential to evolve, so the expected performance enhancement in a tapered FEL is not achieved. We note, however, that for longer pulses it has been found that FEL oscillators can benefit from taper [5,12].

ACKNOWLEDGMENTS

The authors would like to thank the technical staff at Jefferson Lab, especially R. Hill, K. Jordan, and J. Coleman for work on the slit scanner. This work was supported by the Naval Postgraduate School, the Office of Naval Research, the Commonwealth of Virginia, the Laser Processing Consortium, and the U.S. Department of Energy under Contract No. AC05-84-ER40150.

[1] P. L. Morton, Phys. Quantum Electron. **8**, 1 (1981).
[2] N. M. Kroll, P. L. Morton, and M. N. Rosenbluth, IEEE J. Quantum Electron. **QE-17**, 1436 (1981).
[3] N. M. Kroll, P. L. Morton, and M. N. Rosenbluth, Phys. Quantum Electron. **7**, 104 (1979).
[4] J. A. Edighoffer, G. R. Neil, C. E. Hess, T. I. Smith, S. W. Fornaca, and H. A. Schwettman, Phys. Rev. Lett. **52**, 344 (1984).
[5] R. W. Warren, B. E. Newman, J. G. Winston, W. E. Stein, L. M. Young, and C. A. Brau, IEEE J. Quantum Electron. **QE-19**, 391 (1983).
[6] D. A. Jaroszynski *et al.*, Nucl. Instrum. Methods Phys. Res. A **358**, 228 (1995).
[7] E. L. Saldin, E. A. Shneidmiller, and M. V. Yurkov, Opt. Commun. **103**, 297 (1993); Nucl. Instrum. Methods Phys. Res. A **375**, 336 (1996).
[8] G. R. Neil, C. L. Bohn, S. V. Benson, G. Biallas, D. Douglas, H. F. Dylla, R. Evans, J. Fugitt, A. Grippo, J. Gubeli, R. Hill, K. Jordan, R. Li, L. Merminga, P. Piot, J. Preble, M. Shinn, T. Siggins, R. Walker, and B. Yunn, Phys. Rev. Lett. **84**, 662 (2000).
[9] W. B. Colson, in *Laser Handbook*, edited by W. B. Colson, C. Pelligrini, and A. Renieri (North-Holland, Amsterdam, 1990), Vol. 6, Chap. 5.
[10] G. Cord, W. B. Colson, and J. Frisch, Nucl. Instrum. Methods Phys. Res. A **304**, 601 (1991); N. Piovella, P. Chaix, G. Shvets, and D. A. Jaroszynski, Phys. Rev. E **52**, 5470 (1995).
[11] S. Benson *et al.*, Nucl. Instrum. Methods Phys. Res. A **429**, 27 (1999).
[12] F. G. Yee, T. C. Marshall, and S. P. Schlesinger, Nucl. Instrum. Methods Phys. Res. A **272**, 162 (1988).